

# Kosterlitz-Thouless and Gaussian criticalities in a mixed spin- $(\frac{1}{2}, \frac{5}{2}, \frac{1}{2})$ Heisenberg branched chain with exchange anisotropy

Luan M. Veríssimo,<sup>1</sup> Maria S. S. Pereira,<sup>1</sup> Jozef Strečka,<sup>2</sup> and Marcelo L. Lyra<sup>1</sup>

<sup>1</sup>*Instituto de Física, Universidade Federal de Alagoas 57072-970 Maceió-AL, Brazil*

<sup>2</sup>*Department of Theoretical Physics and Astrophysics, Faculty of Science, P. J. Šafárik University, Park Angelinum 9, 040 01 Košice, Slovakia*



(Received 28 January 2019; published 3 April 2019)

Density-matrix renormalization group calculations are used to determine the ground-state phase diagram of the mixed spin- $(1/2, 5/2, 1/2)$  Heisenberg chain whose backbone consists of regularly alternating  $s = 1/2$  and  $S = 5/2$  spins, the latter of which are coupled to additional  $s = 1/2$  spins providing lateral branching. The proposed magnetic structure aims to describe the main characteristics of the heterotrimetallic coordination polymer  $[\text{Cu}^{\text{II}}\text{Mn}^{\text{II}}(\text{L}^1)][\text{Fe}^{\text{III}}(\text{bpb})(\text{CN})_2] \cdot \text{ClO}_4 \cdot \text{H}_2\text{O}$ . The full ground-state phase diagram in the parameter space exchange anisotropy versus magnetic field unveils special critical points, at which the intermediate magnetization plateaus emergent at  $3/7$  and  $5/7$  of the saturation magnetization vanish. A detailed description of the zero-temperature magnetization process and pair entanglement entropy is accomplished with the aim to distinguish the main coupling regimes. A scaling analysis is performed to accurately locate Kosterlitz-Thouless and Gaussian critical points. In particular, we introduce a new finite-size scaling protocol to properly extract the critical parameters from the size dependence of the magnetic-field range corresponding to the magnetization plateau in the close vicinity of the Gaussian point at which two gapped phases meet.

DOI: [10.1103/PhysRevB.99.134408](https://doi.org/10.1103/PhysRevB.99.134408)

## I. INTRODUCTION

Recent advances in a targeted design of single-chain magnets (SCMs) have impelled studies of diverse one-dimensional quantum spin models. In particular, heterobimetallic SCMs [1–4] are nowadays considered as important physical realizations of quantum ferrimagnetic chains, which may exhibit a lot of unconventional magnetic properties at low temperatures due to coexistence of ferro- and antiferromagnetic spin-wave excitations [5–11]. Owing to a slow magnetic relaxation and strong quantum correlations between constituent spin units, SCMs afford a promising class of advanced materials that may be beneficial for the development of spintronics, quantum computing and high-density storage devices [12–16].

The simplest quantum ferrimagnetic spin system is the mixed spin- $(1/2, 1)$  Heisenberg chain. Besides the gapless Tomonaga-Luttinger spin-liquid phase, this one-dimensional quantum spin system displays in a zero-temperature magnetization curve an intermediate plateau at  $1/3$  of the saturation magnetization in agreement with Oshikawa, Yamanaka, and Affleck (OYA) arguments [17]. In the case of an isotropic Heisenberg coupling, the Lieb-Mattis ferrimagnetic phase pertinent to the intermediate  $1/3$ -plateau predominates at low magnetic fields and it terminates at a field-driven quantum phase transition towards the Tomonaga-Luttinger spin-liquid phase emergent at higher magnetic fields [10]. However, it has been recently verified that an exchange anisotropy can suppress the intermediate  $1/3$ -plateau with the character of Lieb-Mattis ferrimagnetic phase through an extension of the spin-liquid regime, until the  $1/3$ -plateau phase ultimately disappears at a special Kosterlitz-Thouless critical point [18,19].

Over the past few decades, experimental realizations of ferrimagnetic quantum Heisenberg chains with alternating spins of different magnitudes have been examined in particular [20]. Heterobimetallic polymeric compounds incorporating regularly alternating  $\text{Cu}^{2+}$  and  $\text{Mn}^{2+}$  magnetic ions, which are linked through dithioxalato ligand, afford for instance experimental realizations of the ferrimagnetic mixed spin- $(1/2, 5/2)$  Heisenberg chains with almost isotropic coupling [1,2]. The OYA criterion predicts for this class of magnetic materials an intermediate magnetization plateau at  $2/3$  of the saturation magnetization [10]. Another interesting class of polymeric compounds affording the ferrimagnetic Heisenberg spin chains constitute metal-organic frameworks, where transition-metal ions such as  $\text{Mn}^{2+}$  are coupled to organic radicals such as nitroxide [21]. Among these, the ferrimagnetic compound  $[\text{Mn}(\text{NITIm})(\text{NITImH})]\text{ClO}_4$  involves alternating sequence of  $\text{Mn}^{2+}$  ions ( $S = 5/2$ ) coupled within the linear chain to the nitroxide radical ( $s = 1/2$ ), whereas additional nitroxide radical is laterally attached to each  $\text{Mn}^{2+}$  ion [22]. According to the OYA criterion, the aforescribed quantum spin chain may exhibit two intermediate magnetization plateaus at  $3/7$  and  $5/7$  of the saturation magnetization even though numerical results unveiled presence of a single  $3/7$  magnetization plateau only [9]. Unconventional magnetic properties have also been recently reported for the ferrimagnetic mixed spin- $(1/2, 1)$  Heisenberg branched chain with the spin-1 pendants [23].

Another strategy for producing the ferrimagnetic Heisenberg spin chains may take advantage of cyanide and organic phenolate bridging ligands to couple diverse metallic ions [24–26]. For instance, the heterotrimetallic coordination compound  $[\text{Cu}^{\text{II}}\text{Mn}^{\text{II}}(\text{L}^1)][\text{Fe}^{\text{III}}(\text{bpb})(\text{CN})_2] \cdot \text{ClO}_4 \cdot \text{H}_2\text{O}$  involves within the main chain superexchange pathways

between  $\text{Fe}^{3+}$  ( $s = 1/2$ ) and  $\text{Mn}^{2+}$  ( $S = 5/2$ ) ions mediated through the cyanide bridge in addition to the lateral superexchange pathways between  $\text{Mn}^{2+}$  ( $S = 5/2$ ) and  $\text{Cu}^{2+}$  ( $s = 1/2$ ) ions mediated by the phenolate bridge [27]. The low-spin  $\text{Fe}^{3+}$  ion has a strong uniaxial magnetic anisotropy due to unquenched orbital momentum and hence, the superexchange coupling between  $\text{Fe}^{3+}$  and  $\text{Mn}^{2+}$  ions along the chain backbone should be highly anisotropic in contrast to the lateral superexchange coupling between  $\text{Mn}^{2+}$  and  $\text{Cu}^{2+}$  ions that should be nearly isotropic. Considering that the exchange anisotropy can significantly affect the nature of quantum ground states and phase transitions, it is of principal importance to investigate its effect upon the ground state of this heterotrimetallic coordination compound.

In the present work, we will therefore address the above question by reporting a detailed density-matrix renormalization group (DMRG) study of the ground state of a mixed spin-(1/2, 5/2, 1/2) Heisenberg branched chain accounting for the exchange anisotropy between  $s = 1/2$  and  $S = 5/2$  spins coupled along the chain backbone. We will provide results for the magnetic-field dependence of the sublattice magnetization of each spin species, the total magnetization and the entanglement entropy between the laterally coupled spins. By exploring distinct anisotropy regimes, we will unveil the full ground-state phase diagram involving three different gapped ground states corresponding to the intermediate magnetization plateaus, as well as, two special quantum critical points at which the intermediate magnetization plateaus disappear. A finite-size scaling analysis will be used to characterize the distinct nature of these quantum critical points.

## II. MIXED SPIN-(1/2, 5/2, 1/2) HEISENBERG BRANCHED CHAIN

The essential magnetic interactions of the heterotrimetallic polymeric compound  $[\text{Cu}^{\text{II}}\text{Mn}^{\text{II}}(\text{L}^1)][\text{Fe}^{\text{III}}(\text{bpb})(\text{CN})_2] \cdot \text{ClO}_4 \cdot \text{H}_2\text{O}$  [27] can be captured by the mixed spin-(1/2, 5/2, 1/2) Heisenberg branched chain with three distinct spins per unit cell resembling crystallographic positions of  $\text{Fe}^{3+}$ ,  $\text{Mn}^{2+}$ , and  $\text{Cu}^{2+}$  magnetic ions, respectively (see Fig. 1 for a schematic illustration). The magnetic backbone of the considered quantum spin chain consists of an alternating sequence of  $s = 1/2$  and  $S = 5/2$  spins resembling  $\text{Fe}^{3+}$  and  $\text{Mn}^{2+}$  ions, which interact through the anisotropic XXZ Heisenberg exchange coupling due to a relatively high unquenched orbital momentum of  $\text{Fe}^{3+}$  ions residing a low-spin state  $s = 1/2$ . Contrary to this, each  $\text{Mn}^{2+}$  ion of the magnetic backbone is laterally attached via the isotropic Heisenberg coupling to  $\text{Cu}^{2+}$  ion with  $s = 1/2$  spin. The Hamiltonian of the underlying mixed spin-(1/2, 5/2, 1/2) Heisenberg branched chain can be written as

$$\mathcal{H} = J \sum_{i=1}^{N_c} [(\mathbf{s}_{1,i} \cdot \mathbf{S}_{2,i})_{\Delta} + (\mathbf{s}_{1,i+1} \cdot \mathbf{S}_{2,i})_{\Delta}] + J' \sum_{i=1}^{N_c} \mathbf{S}_{2,i} \cdot \mathbf{s}_{3,i} - g\mu_B B \sum_{i=1}^{N_c} (s_{1,i}^z + S_{2,i}^z + s_{3,i}^z), \quad (1)$$

where  $\mathbf{s}_{1,i}$  stands for the  $s = 1/2$  spin of  $\text{Fe}^{3+}$  ion,  $\mathbf{S}_{2,i}$  corresponds to the  $S = 5/2$  spin of  $\text{Mn}^{2+}$  ion and  $\mathbf{s}_{3,i}$  to the

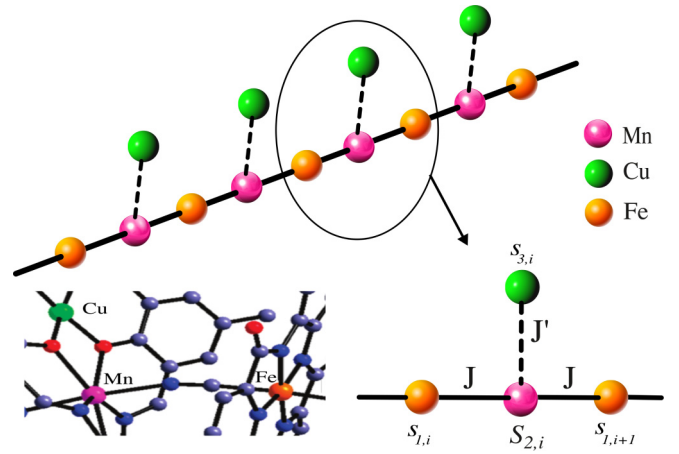


FIG. 1. The magnetic structure of the mixed spin-(1/2, 5/2, 1/2) Heisenberg branched chain, which mimics the main characteristics of the heterotrimetallic polymeric compound  $[\text{Cu}^{\text{II}}\text{Mn}^{\text{II}}(\text{L}^1)][\text{Fe}^{\text{III}}(\text{bpb})(\text{CN})_2] \cdot \text{ClO}_4 \cdot \text{H}_2\text{O}$  [27]. The backbone of the polymeric chain consists of alternating sequence of  $s = 1/2$  and  $S = 5/2$  spins pertinent to  $\text{Fe}^{3+}$  and  $\text{Mn}^{2+}$  magnetic ions, whereas an additional pendant  $s = 1/2$  spin inherent to  $\text{Cu}^{2+}$  ion is attached to each  $S = 5/2$  spin ( $\text{Mn}^{2+}$  ion) of the backbone. The lateral coupling  $J'$  is considered as the isotropic Heisenberg interaction, while the coupling constant  $J$  along the backbone is considered as the XXZ anisotropic Heisenberg interaction.

$s = 1/2$  spin of  $\text{Cu}^{2+}$  ion laterally attached to the backbone. Hence, the coupling constant  $J'$  determines the strength of the isotropic exchange interaction in the lateral direction, while the exchange constant  $J$  accounts for the anisotropic XXZ exchange interaction along the chain backbone

$$(\mathbf{s}_{1,i} \cdot \mathbf{S}_{2,i})_{\Delta} = s_{1,i}^x S_{2,i}^x + s_{1,i}^y S_{2,i}^y + \Delta s_{1,i}^z S_{2,i}^z. \quad (2)$$

Note furthermore that the parameter  $\Delta$  quantifies the degree of anisotropy in the XXZ exchange interaction along the main chain axis,  $B$  is the external magnetic field oriented along the  $z$  axis,  $\mu_B$  is the Bohr magneton and  $g$  is the gyromagnetic factor, which is assumed to be the same for all three metallic species for the sake of simplicity. In this way, the anisotropy parameter  $\Delta$  also measures the relative strength between the coupling constants within the longitudinal and transverse directions. In what follows, we will be mainly interested in the effects of the degree of exchange anisotropy on the ground-state phase diagram and quantum phase transition by restricting our further attention to the particular case with  $J = J'$ , which will henceforth serve as the energy unit. We will also use units of  $g\mu_B = 1$ .

## III. DMRG RESULTS FOR THE GROUND-STATE PROPERTIES

The ground-state energy, entanglement entropy, global and local magnetizations of the mixed spin-(1/2, 5/2, 1/2) Heisenberg branched chain were calculated using state-of-the-art DMRG simulations by adapting the open-source software from the Algorithms and Libraries for Physics Simulations (ALPS) project [28]. To this aim, the periodic boundary conditions were imposed in order to reduce finite-size effects,

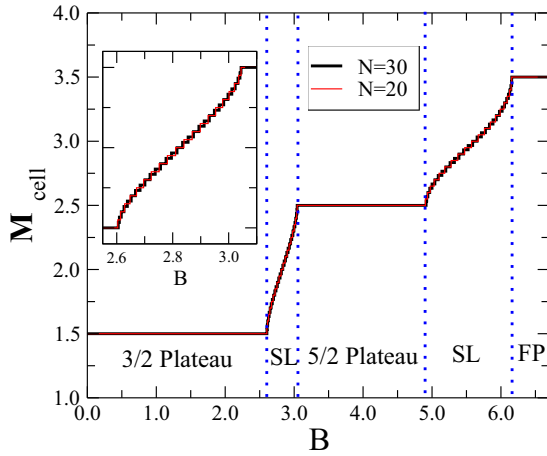


FIG. 2. The total magnetization per unit cell as a function of the external magnetic field for the fully isotropic mixed spin-(1/2, 5/2, 1/2) Heisenberg branched chain with  $\Delta = 1$ . Data for two chain sizes are reported to show the absence of significant finite-size corrections. These are mainly reflected in the number of magnetization steps within the spin-liquid phase (see inset). The intermediate magnetization plateaus at the total magnetizations 3/2 and 5/2 per unit cell are detected besides the ultimate fully polarized (FP) ferromagnetic phase. The field-driven quantum phase transitions, which are delimited by dotted vertical lines, separate gapful ground states from the gapless Tomonaga-Luttinger spin-liquid (SL) phase.

whereas the number of kept states during the DMRG simulations was set up to 800 with eight sweeps for the targeted system size. This setting enabled us to achieve convergence of the ground-state energy and magnetization with a truncation error of  $10^{-8}$  and an absolute accuracy in energies of  $10^{-4}$  (relative error of  $10^{-8}$ ) for the mixed spin-(1/2, 5/2, 1/2) Heisenberg branched chains. Simulations were mainly performed in chains with  $N = 30$  unit cells, with somewhat larger chains being simulated in a vicinity of special critical points.

Let us start our discussion by exploring the magnetization curve of the fully isotropic mixed spin-(1/2, 5/2, 1/2) Heisenberg branched chain with  $\Delta = 1$ . For this purpose, the total magnetization per unit cell is plotted in Fig. 2 as a function of the external magnetic field, which invokes presence of two intermediate magnetization plateaus with the total magnetization  $M_{\text{cell}} = 3/2$  and  $5/2$  per unit cell. If the total magnetization per unit cell would be normalized with respect to its saturation value, the observed magnetization plateaus would correspond to  $M_{\text{cell}}/M_s = 3/7$  and  $5/7$  in agreement with OYA criterion. It is noteworthy that the magnetization plateau with the total magnetization  $M_{\text{cell}} = 3/2$  per unit cell develops from very low magnetic fields in accordance with the Lieb-Mattis theorem [29]. A comparison between the magnetization data computed for  $N = 20$  and  $N = 30$  unit cells implies absence of relevant finite-size effects on essential features of the magnetization curves (see Fig. 2), since both system sizes afford roughly the same magnetization curves and critical fields.

In order to provide a deeper insight into the magnetic ordering realized within each phase, we have also computed the magnetic-field dependence of the mean values of all

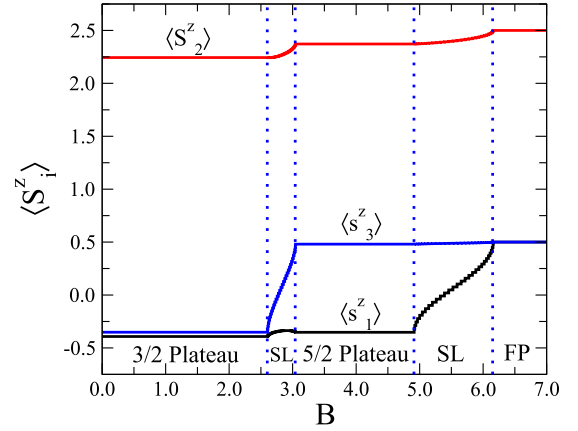


FIG. 3. The mean values of all individual spin species emergent in the unit cell of the fully isotropic mixed spin-(1/2, 5/2, 1/2) Heisenberg branched chain with  $\Delta = 1$ . There is a two-step transition towards the full saturation when the magnetic field predominantly reverses within the first (second) spin-liquid region the lateral spins  $s_3$  (the backbone spins  $s_1$ ). The numerical data stem from DMRG simulations of spin chains with  $N = 30$  unit cells.

individual spin species emergent in the unit cell of the isotropic mixed spin-(1/2, 5/2, 1/2) Heisenberg branched chain (see Fig. 3). It is evident from Fig. 3 that the large spin species  $S = 5/2$  are in all phases predominantly oriented along the magnetic field though quantum fluctuations prevent its full polarization except of the ultimate fully polarized state emergent above the saturation field. At low magnetic fields, both smaller spins  $s = 1/2$  are predominantly oriented against the magnetic field due to the antiferromagnetic coupling with the large spin  $S = 5/2$  within the Lieb-Mattis ferrimagnetic phase manifested as the intermediate plateau with the total magnetization  $M_{\text{cell}} = 3/2$  per unit cell. It should be also stressed, however, that the mean values of the individual spin species are not fully saturated within the Lieb-Mattis ferrimagnetic ground state due to quantum fluctuations, which are responsible for a quantum reduction of the magnetization for all three spin species. It turns out, moreover, that the laterally attached spins  $s = 1/2$  ( $s_3$ ) tend to align towards the magnetic field before the backbone spins  $s_1$  within the lower range of magnetic fields, which follows after a field-driven quantum phase transition between the gapful Lieb-Mattis ferrimagnetic phase and the gapless Tomonaga-Luttinger spin-liquid phase. The laterally attached spins successively become almost perfectly aligned along the magnetic field within another quantum ferrimagnetic ground state, which is responsible for the intermediate plateau with the total magnetization  $M_{\text{cell}} = 5/2$  per unit cell. Last but not least, the backbone spins  $s = 1/2$  ( $s_1$ ) from the main chain undergo a gradual spin reorientation within the second spin-liquid region, which appears above a field-induced quantum phase transition closely associated with a breakdown of the intermediate plateau with the total magnetization  $M_{\text{cell}} = 5/2$  per unit cell. Interestingly, the magnetization of the backbone spins  $s_1$  from the main chain exhibit a nonmonotonous dependence during the spin reorientation of the lateral spins  $s_3$ .

It is quite obvious from the unsaturated character of the local magnetizations (mean spin values) that all

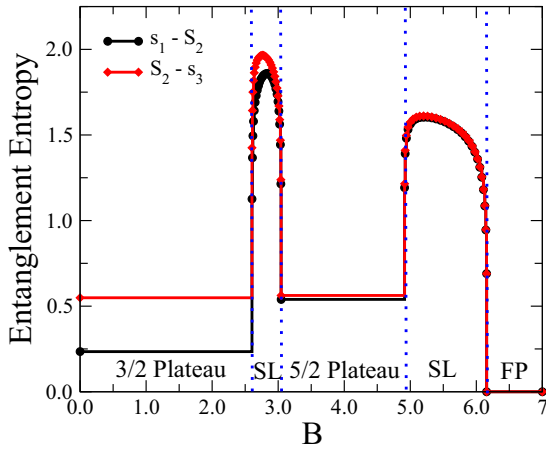


FIG. 4. The magnetic-field dependence of von Neumann entanglement entropy between the large  $S = 5/2$  spin species ( $S_2$ ) and either the laterally coupled spins ( $s_3$ ) or the backbone spins ( $s_1$ ) of the fully isotropic mixed spin-(1/2, 5/2, 1/2) Heisenberg branched chain with  $\Delta = 1$ . The pair entanglement entropies pass through maxima during the spin reversal emergent within the spin-liquid phases. The numerical data stem from DMRG simulations of spin chains with  $N = 30$  unit cells.

aforedescribed ground states except the fully polarized phase emergent above the saturation field should display a high degree of quantum entanglement. There are several quantities that are commonly used to analyze the degree of quantum entanglement. In what follows, we will illustrate this aspect by computing von Neumann entropy, which sheds light on the entanglement of a spin pair with the remaining part of the system [30–32]. In particular, we will focus on the pair von Neumann entropy of the large spin  $S_2$  ( $S = 5/2$ ) with one of its nearest neighbors  $s_1$  or  $s_3$  ( $s = 1/2$ ). Both pair von Neumann entropies are plotted in Fig. 4 against the magnetic field for the fully isotropic mixed spin-(1/2, 5/2, 1/2) Heisenberg branched chain with  $\Delta = 1$ . Within both plateau phases, the pair von Neumann entropies remain constant and, as expected, they vanish in the classical fully polarized state. In the Lieb-Mattis ferrimagnetic phase ( $M_{\text{cell}} = 3/2$  plateau), the pair von Neumann entropy of the large spin  $S = 5/2$  with the laterally attached spin  $s_3$  is larger than that with the neighboring backbone spin  $s_1$ . The reversal of the lateral spin  $s_3$  within another quantum ferrimagnetic phase ( $M_{\text{cell}} = 5/2$  plateau) has just a small impact on the  $S_2 - s_3$  pair entanglement entropy, while it significantly enhances the pair entanglement entropy  $s_1 - S_2$  (both pair entanglement entropies become nearly the same). It is noteworthy that the pair von Neumann entropies reach local maxima within the spin-liquid region, which are closely related to both spin-reversal processes. This feature is related to the development of strong quantum correlations in the spin-liquid phases. The maximum values of the pair entanglement entropies can be detected during the reversal of the lateral spin  $s_3$ .

In addition, we have also performed an extensive study of the ground-state properties of the mixed spin-(1/2, 5/2, 1/2) Heisenberg branched chain for a wide range of values of the exchange anisotropy  $\Delta$ . First, we will report some results for one representative case with the anisotropy parameter

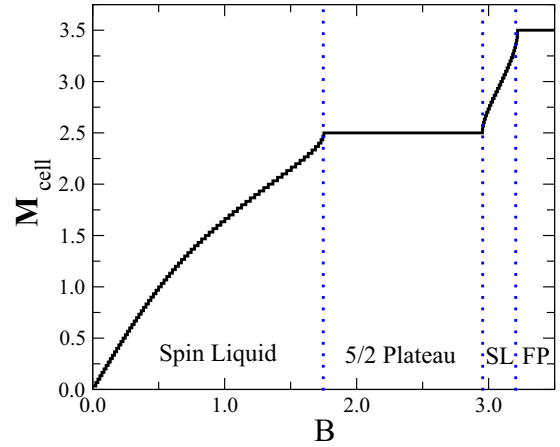


FIG. 5. The total magnetization per unit cell as a function of the external magnetic field for the mixed spin-(1/2, 5/2, 1/2) Heisenberg branched chain with an anisotropic XXZ interaction along the backbone characterized through the exchange anisotropy  $\Delta = -0.2$ . Only the intermediate magnetization plateau at the total magnetization  $M_{\text{cell}} = 5/2$  per unit cell is present at moderate values of the magnetic field. The field-driven quantum phase transitions are delimited by dotted vertical lines. The numerical data stem from DMRG simulations of spin chains with  $N = 30$  unit cells.

$\Delta = -0.2$ . Under this condition, the coupling between the longitudinal spin components along the backbone chain is much weaker than that between the transverse ones while having the reverse ferromagnetic character. In contrast to the previously discussed case with isotropic coupling ( $\Delta = 1.0$ ), the spin-liquid phase develops in the zero-temperature magnetization curve at low magnetic fields instead of the Lieb-Mattis ferrimagnetic phase (see Fig. 5). Owing to this fact, an intermediate plateau with the total magnetization  $M_{\text{cell}} = 3/2$  per unit cell is not evident in the magnetization curve, which involves just one wide intermediate magnetization plateau with the total magnetization  $M_{\text{cell}} = 5/2$  per unit cell. Besides, it directly follows from Fig. 6 that the observed magnetization plateau has completely different nature than the one reported previously for the same value of the total magnetization  $M_{\text{cell}} = 5/2$  per unit cell. In this particular case, the backbone spins  $s_1$  are predominantly aligned into the magnetic field, while the lateral spins  $s_3$  are predominantly aligned in opposite to the magnetic field due to the antiferromagnetic coupling with the field-aligned large spins  $S_2$ . Such ordering of spins directly relates to a weak ferromagnetic coupling between the longitudinal spin components along the backbone of the main chain.

To examine the degree of quantum entanglement, we have plotted in Fig. 7 the magnetic-field dependence of the pair von Neumann entropies for the highly anisotropic mixed spin-(1/2, 5/2, 1/2) Heisenberg branched chain with a weak ferromagnetic longitudinal coupling  $\Delta = -0.2$ . These results would suggest that the quantum entanglement characterized through the pair von Neumann entropies is generally lowered within the first spin-liquid region upon strengthening of the magnetic field until it approaches the constant local minimum, which is then stable over the magnetic-field range corresponding to the intermediate plateau with the total magnetization



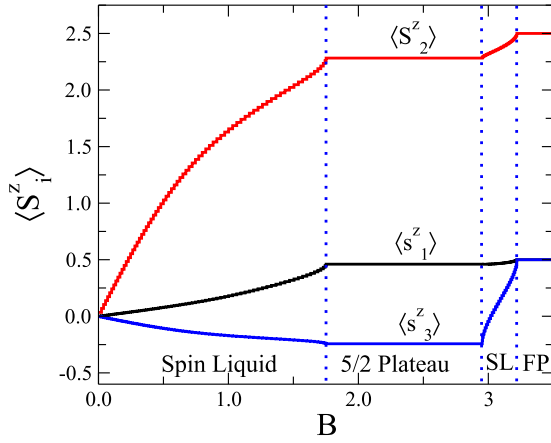


FIG. 6. The mean values of all individual spin species emergent in the unit cell of the mixed spin-(1/2, 5/2, 1/2) Heisenberg branched chain with an anisotropic XXZ interaction along the backbone chain with  $\Delta = -0.2$ . The spins  $s_1$  and  $S_2$  from the backbone chain are predominantly oriented along the magnetic field, while the lateral spins  $s_3$  are predominantly ordered in opposite to the magnetic field within the intermediate plateau with the total magnetization  $M_{\text{cell}} = 5/2$  per unit cell, which breaks down at a field-induced quantum phase transitions towards the spin-liquid phase associated with a reversal of the lateral spins  $s_3$ . The numerical data stem from DMRG simulations of spin chains with  $N = 30$  unit cells.

$M_{\text{cell}} = 5/2$  per unit cell. It should be emphasized that the maximum value of the pair entropy  $S_2 - s_3$  is relatively close to the limiting value of a spin pair (1/2, 5/2) (i.e.,  $\ln 12 \approx 4.4849$ ), which indicates a strong quantum fluctuations at low enough magnetic fields. Note furthermore that the pair von Neumann entropy between the spins  $S_2 - s_3$  remains larger than the pair von Neumann entropy between spins  $s_1 - S_2$  regardless of a relative size of the magnetic field in contrast

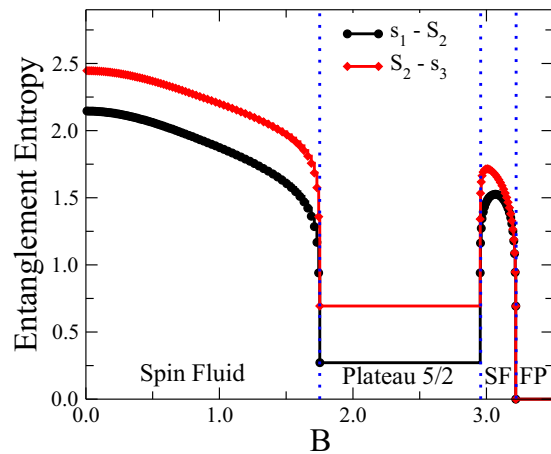


FIG. 7. The magnetic-field dependence of von Neumann entanglement entropy between the large  $S = 5/2$  spin species ( $S_2$ ) and either the laterally coupled spins ( $s_3$ ) or the backbone spins ( $s_1$ ) of the highly anisotropic mixed spin-(1/2, 5/2, 1/2) Heisenberg branched chain with the exchange anisotropy  $\Delta = -0.2$ . The pair entanglement entropies approach maximal values at zero magnetic field. The numerical data stem from DMRG simulations of spin chains with  $N = 30$  unit cells.

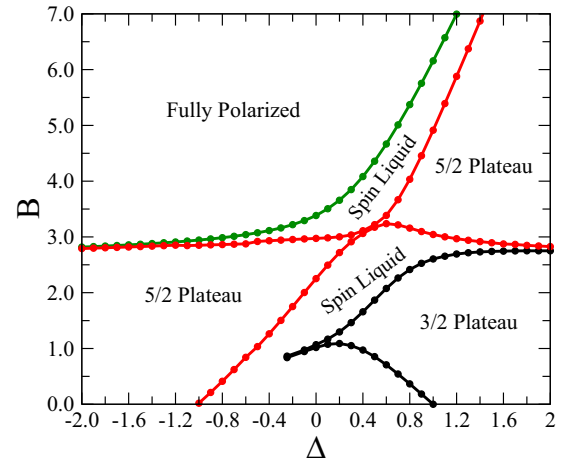


FIG. 8. The ground-state phase diagram of the mixed spin-(1/2, 5/2, 1/2) Heisenberg branched chain in the exchange anisotropy vs magnetic field ( $\Delta - B$ ) plane. There exist two distinct 5/2-plateau phases, which merge together at the Gaussian critical point. The intermediate 3/2-plateau pertinent to the Lieb-Mattis ferrimagnetic phase terminates at the Kosterlitz-Thouless critical point. The plateau phases are separated from each other through the spin-liquid regions.

with the behavior thoroughly described for the fully isotropic case. It is interesting to notice that, in both cases of isotropic and anisotropic interactions, the pair entropy of  $s_1 - S_2$  is substantially smaller than that for the  $s_3 - S_2$  pair if  $s_3$  and  $S_2$  have average opposite orientations (see the 3/2 plateau in Fig. 4 and the 5/2 plateau in Fig. 7). This feature indicates that antiferromagnetic transversal correlations effectively reduces the degree of quantum entanglement along the chain. For ferromagnetic transversal correlations, both pair entropies are of similar magnitudes (see 5/2 plateau in Fig. 4).

Finally, let us conclude our survey of the results by a comprehensive analysis of the ground-state phase diagram of the mixed spin-(1/2, 5/2, 1/2) Heisenberg branched chain, which has been constructed in the exchange anisotropy versus magnetic field ( $\Delta - B$ ) plane from zero-temperature magnetization curves calculated for the following range of the anisotropy parameter  $\Delta \in [-2, 2]$ . The phase boundaries correspond to the lower and upper magnetic fields of each plateau phase. It is quite evident from Fig. 8 that the overall ground-state phase diagram totally involves a single 3/2-plateau phase and two distinct 5/2-plateau phases besides the gapless Tomonaga-Luttinger spin-liquid phase and the fully polarized ferromagnetic phase. The intermediate 3/2-plateau relates to the Lieb-Mattis ferrimagnetic phase, which appears at low enough magnetic fields whenever the coupling between the longitudinal spin components along the backbone is strong antiferromagnetic ( $\Delta > 1$ ). Contrary to this, the weak coupling  $|\Delta| < 1$  between the longitudinal spin components of either ferromagnetic ( $\Delta < 0$ ) or antiferromagnetic ( $\Delta > 0$ ) character supports the presence of the quantum spin-liquid phase at low enough magnetic fields though the 3/2-plateau phase may still be found at moderate values of the magnetic field. However, the width of the 3/2-plateau phase substantially shrinks upon lowering of the anisotropy parameter  $\Delta$  until it completely vanishes at the Kosterlitz-Thouless critical point

$\Delta_c = -0.247$ . The Kosterlitz-Thouless nature of this special point represents the transition from a gapped (massive) phase on which there is a magnetization plateau to a nongapped (nonmassive) critical spin-liquid phase. The strong ferromagnetic coupling  $\Delta < -1$  between the longitudinal spin components along the backbone causes the existence of the 5/2-plateau phase at sufficiently low magnetic fields, in which the backbone spins  $s_1$  and  $S_2$  are predominantly oriented into the magnetic field and the lateral spins  $s_3$  against the magnetic field. This is in a sharp contrast with the spin arrangement of the second 5/2-plateau phase, which emerges at relatively higher magnetic fields whenever stronger antiferromagnetic coupling between the longitudinal spin components along the backbone is considered. The latter 5/2-plateau phase is consistent the quantum ferrimagnetic order of the backbone spins  $s_1$  and  $S_2$  supplemented with almost polarized lateral spins  $s_3$ . The two 5/2-plateau phases meet together at a very special Gaussian critical point, which implies absence of the intermediate 5/2-plateau for one particular value of the exchange anisotropy  $\Delta_c = 0.467$ . It should be mentioned that all three quantum ferrimagnetic phases being responsible for the emergence of intermediate magnetization plateaus are separated by continuous quantum phase transitions from the Tomonaga-Luttinger spin-liquid phase, which is generally suppressed for very large values of the exchange anisotropy  $\Delta$  because a strong ferro- or antiferromagnetic coupling between the longitudinal spin components along the backbone chain suppresses quantum fluctuations being a necessary prerequisite of the quantum spin-liquid ground states.

To precisely locate the ending points of the gapped 3/2- and 5/2-plateau phases, we have performed a finite-size scaling analysis for the width of each intermediate magnetization plateau in the close vicinity of both quantum critical points. If the zero-temperature magnetization curve involves a true magnetization plateau, then, the plateau should persist in a range of the magnetic fields  $\Delta B = B^+ - B^-$  ( $B^+$  and  $B^-$  are the upper and lower critical fields delimiting the plateau) and this field range should remain finite as the chain size  $N$  increases. On the other hand, the range of each magnetization sector should scale as  $1/N$  when this magnetization sector is not responsible for a persistent magnetization plateau. Therefore, when  $N\Delta B$  curves for a given magnetization sector are plotted against the control parameter  $\Delta$  for distinct chain sizes, they should merge together in absence of the actual magnetization plateau, in contrast to a continuously increase with the system size  $N$  observable within the gapful plateau phases.

Let us start our finite-size scaling analysis by plotting  $N\Delta B$  against the anisotropy parameter  $\Delta$  in a vicinity of the Kosterlitz-Thouless (KT) critical point, at which the intermediate 3/2-plateau vanishes. It can be clearly seen from Fig. 9(a) that the  $N\Delta B$  curves plotted for distinct chain sizes collapse within the spin-liquid phase and start to diverge above the KT critical point. However, the exponentially small size of the plateau near the KT point makes difficult to locate the KT critical point using DMRG data, which were obtained for relatively small chain sizes. To give a more precise estimate of the KT critical point, we have also explored the expected universal scaling form of the plateau size  $N\Delta B = f(\xi/N)$ , where the correlation length  $\xi$  should

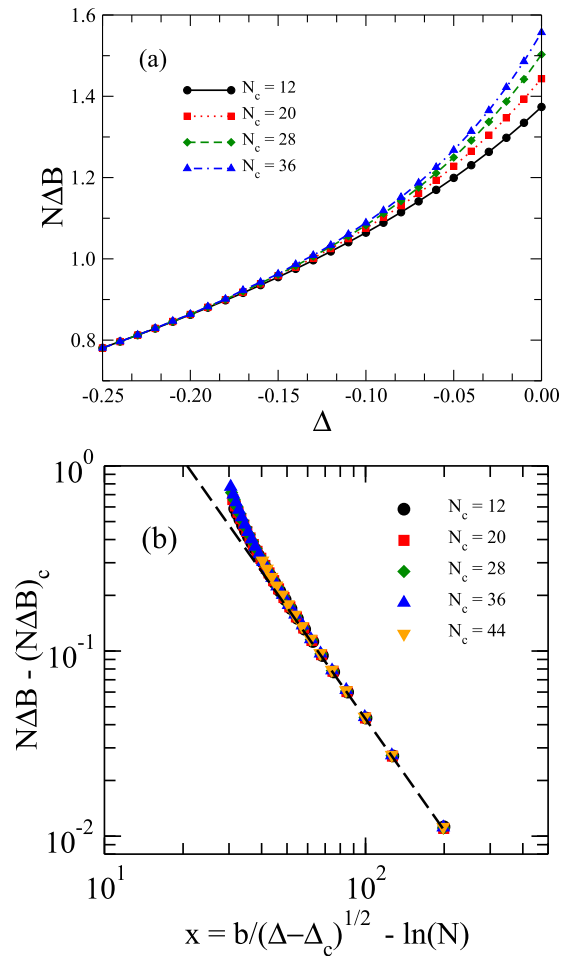


FIG. 9. (a) A plot of  $N\Delta B$  data for the magnetization sector being responsible for the 3/2-plateau against the anisotropy parameter  $\Delta$  in a vicinity of the KT critical point. All curves collapse within the spin-liquid phase but diverge in the 3/2-plateau phase. (b) The  $N\Delta B - (N\Delta B)_c$  data as a function of the proper scaling variable  $x = b/(\Delta - \Delta_c)^{1/2} - \ln N$ . The best data collapse is achieved for  $\Delta_c = -0.247$ . The dashed line represents the large  $x$  behavior  $f(x) \propto 1/x^2$ , which is consistent with the linear behavior of  $N\Delta B$  close to the KT critical point shown in (a).

exhibit an essential singularity when diverging close to the KT point according to  $\xi \propto e^{b/(\Delta - \Delta_c)^{1/2}}$  as long as an eventual small logarithmic correction to scaling is neglected [33,34]. Owing to this fact, all  $N\Delta B$  curves should collapse above the KT critical point when plotted against the proper scaling variable  $x = b/(\Delta - \Delta_c)^{1/2} - \ln N$  with  $b$  being a constant independent of  $\Delta$ . The best data collapse of the  $N\Delta B$  curves was obtained for the exchange anisotropy  $\Delta_c = -0.247$  and is shown in Fig. 9(b). The fine collapse of data supports the absence of relevant logarithmic corrections to scaling. It is worth noticing that the 3/2-plateau cannot be clearly visible in Fig. 5 due to its exponentially small size just above the KT critical point, since it becomes indistinguishable in the reported numerical data from finite-size steps resulting from other magnetization sectors.

Next, let us turn our attention to a finite-size scaling analysis close to the second special quantum critical point, at

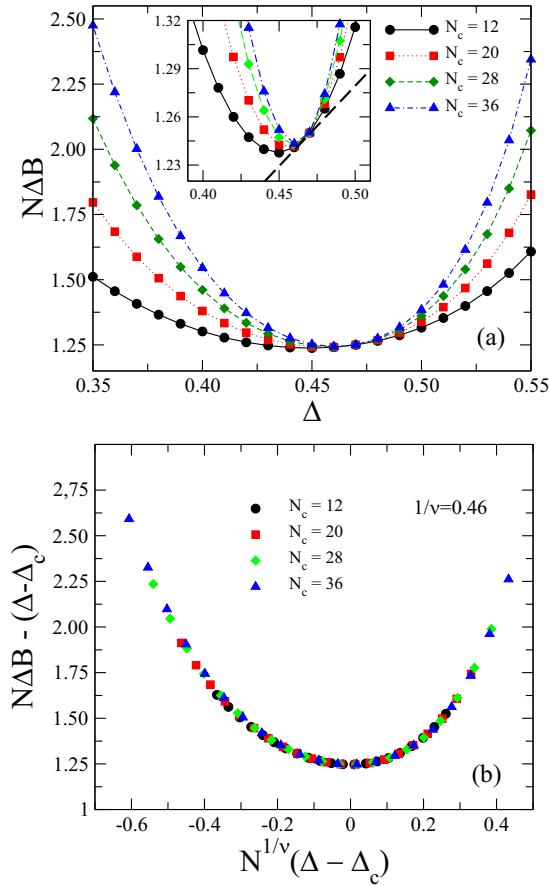


FIG. 10. (a) A plot of  $N\Delta B$  data for the magnetization sector being responsible for the 5/2-plateau against the anisotropy parameter  $\Delta$  in a vicinity of the Gaussian critical point. All displayed curves coalesce at the Gaussian critical point  $\Delta_c$ , where they have unitary slope (see the inset). (b) The  $N\Delta B - (\Delta - \Delta_c)$  data as a function of the proper scaling variable  $x = N^{1/\nu}(\Delta - \Delta_c)$ . The best data collapse is achieved for  $\Delta_c = 0.467$  and  $1/\nu = 0.46$ .

which two different 5/2-plateau phases meet together. Such Gaussian critical point is commonly observed in anisotropic quantum Heisenberg spin chains [7,35–37]. The scaled size of the 5/2-plateau  $N\Delta B$  is plotted in Fig. 10(a) as a function of the exchange anisotropy  $\Delta$  for distinct chain sizes. It can be clearly seen from this figure that all displayed curves coalesce at a single point, which can be identified with the Gaussian critical point. In fact, all displayed curves have unitary slope at the Gaussian critical point  $\Delta_c$  and there is no crossing point (see the inset). This feature requires an extended scaling form for  $N\Delta B$  to account for the size independence of the slope at the critical point. The proper scaling format for  $N\Delta B$  near the Gaussian critical point should have the form

$$N\Delta B = (N\Delta B)_c + (\Delta - \Delta_c) + f(\xi/N), \quad (3)$$

because the finite-size scaling should affect only the higher-order terms of its series expansion. The Gaussian critical point has a regular singularity and hence,  $\xi \propto (\Delta - \Delta_c)^{-\nu}$  with  $\nu$  being the critical exponent of the correlation length. This scaling form implies that all curves  $N\Delta B - (\Delta - \Delta_c)$  should collapse into a single curve independent of the chain

size when plotted against  $N^{1/\nu}(\Delta - \Delta_c)$ . Such data collapse is shown in Fig. 10(b), which provides our best estimate for the correlation length critical exponent  $1/\nu = 0.46$ ,  $\Delta_c = 0.467$ , and  $(N\Delta B)_c = 1.246$ . Notice that the above scaling analysis allows to precisely evaluate the critical properties of the Gaussian point using data directly extracted from chains with periodic boundary conditions. As such, it stands as an efficient alternative protocol in comparison with techniques resorting to twisted boundary conditions [36].

#### IV. SUMMARY AND CONCLUSIONS

In summary, we have presented a detailed DMRG study of the ground-state properties of the mixed spin-(1/2, 5/2, 1/2) Heisenberg branched chain, which mimics the main characteristics of the heterotrimetallic coordination polymer  $[\text{Cu}^{\text{II}}\text{Mn}^{\text{II}}(\text{L}^1)][\text{Fe}^{\text{III}}(\text{bpb})(\text{CN})_2] \cdot \text{ClO}_4 \cdot \text{H}_2\text{O}$  [27]. The backbone of the mixed spin-(1/2, 5/2, 1/2) Heisenberg branched chain consists of regularly alternating  $s = 1/2$  and  $S = 5/2$  spins coupled through an anisotropic XXZ exchange interaction, which takes into account the superexchange coupling between the low-spin  $\text{Fe}^{3+}$  ( $s = 1/2$ ) and high-spin  $\text{Mn}^{2+}$  ( $S = 5/2$ ) magnetic ions. The branching of the mixed spin-(1/2, 5/2, 1/2) Heisenberg chain is preserved by an isotropic Heisenberg interaction with the third spin species  $s = 1/2$ , which relates to the lateral superexchange coupling of each  $\text{Mn}^{2+}$  ( $S = 5/2$ ) magnetic ion with the pendant  $\text{Cu}^{2+}$  ( $s = 1/2$ ) magnetic ion. In particular, we have calculated the ground-state phase diagram, global and local magnetizations in addition to von Neumann pair entanglement entropies, which were used for quantifying the degree of quantum entanglement.

It has been demonstrated that the exchange anisotropy has a strong influence upon the ground state of the mixed spin-(1/2, 5/2, 1/2) Heisenberg branched chain. If the backbone coupling between longitudinal spin components is stronger than that between transverse spin components (i.e.,  $|\Delta| > 1$ ), the mixed spin-(1/2, 5/2, 1/2) Heisenberg branched chain exhibits at low enough magnetic fields the gapful ferrimagnetic ground state being responsible either for the intermediate 3/2-plateau ( $\Delta > 1$ ) or 5/2-plateau ( $\Delta < -1$ ) phase. On the other hand, the gapless Tomonaga-Luttinger spin-liquid phase develops at low enough magnetic fields whenever the backbone coupling between longitudinal spin components is weaker than that between transverse spin components (i.e.,  $|\Delta| < 1$ ). Altogether, the mixed spin-(1/2, 5/2, 1/2) Heisenberg branched chain displays two distinct ferrimagnetic 5/2-plateau phases that meet together at the Gaussian critical point in addition to a single ferrimagnetic 3/2-plateau phase of Lieb-Mattis type, which disappears at the Kosterlitz-Thouless critical point. The nature of these two special quantum critical points was corroborated by a comprehensive finite-size scaling analysis. It is also noteworthy that two quantum ferrimagnetic ground states with the same total magnetization  $M_{\text{cell}} = 5/2$  per unit cell differ from each other by the relative orientation of the backbone and lateral spins  $s = 1/2$ . These gapped phases meet at a single Gaussian point at which the gap vanishes. We have unveiled that a proper scaling analysis in a close vicinity of this transition has to take into account the

scale invariance of both rescaled gaps and its gradient at the Gaussian point.

Several recently synthesized bimetallic and trimetallic polymeric coordination compounds have their main superexchange couplings between two spin species forming the backbone chain and a third spin species laterally attached to one of the backbone spins such as one-dimensional manganese-nitroxide [21,22] and heterotrimetallic [27] coordination polymers. These polymeric coordination compounds thus afford ideal physical systems, which can be examined in connection with an experimental probing of unconventional quantum phase transitions and critical points in putative one-dimensional quantum spin systems.

In particular, the available experimental data for the low-temperature magnetization curve of the heterotrimetallic coordination polymer  $[\text{Cu}^{\text{II}}\text{Mn}^{\text{II}}(\text{L}^1)][\text{Fe}^{\text{III}}(\text{bpb})(\text{CN})_2] \cdot \text{ClO}_4 \cdot \text{H}_2\text{O}$  [27] recorded at magnetic fields up to 5-T signals an intermediate plateau roughly at 3/7 of the saturation magnetization (see Fig. S1 in Ref. [27]), i.e., 3/2-plateau when expressed through the magnetization per unit cell in  $g\mu_B$  units. The experimentally detected 3/7-plateau thus corresponds to the quantum ferrimagnetic ground state, which has the spin-5/2 ( $\text{Mn}^{2+}$ ) magnetic ions almost fully aligned towards the magnetic field and both spin-1/2 ( $\text{Fe}^{3+}$  and  $\text{Cu}^{2+}$ ) magnetic ions almost fully aligned in opposite to the magnetic field (see Fig. 3 for typical field dependence of individual magnetic moments). Note furthermore that this magnetization scenario is consistent with the antiferromagnetic nature of both considered coupling constants, which is

also supported by temperature dependence of susceptibility times temperature product (see Fig. 3 in Ref. [27]). The high-field magnetization curve of the heterotrimetallic coordination polymer  $[\text{Cu}^{\text{II}}\text{Mn}^{\text{II}}(\text{L}^1)][\text{Fe}^{\text{III}}(\text{bpb})(\text{CN})_2] \cdot \text{ClO}_4 \cdot \text{H}_2\text{O}$  thus represents a challenging task for future experimental study, because it could possibly involve, according to the ground-state phase diagram shown in Fig. 8, another intermediate 5/7-plateau in addition to two tiny spin-liquid regions even though both coupling constants should be apparently of different relative size. We hope that the complex ground-state phase diagram reported in the present work, which involves two special quantum critical points of Gaussian and Kosterlitz-Thouless types, will stimulate further experimental efforts towards the synthesis and magnetic characterization of this promising class of magnetic materials and motivate additional theoretical works aiming to unveil other exotic magnetic phenomena.

## ACKNOWLEDGMENTS

This work was supported by CAPES (Coordenação de Aperfeiçoamento de Pessoal de Nível Superior), CNPq (Conselho Nacional de Desenvolvimento Científico e Tecnológico), and FAPEAL (Fundação de Apoio à Pesquisa do Estado de Alagoas). J.S. acknowledges financial support by the grant of The Ministry of Education, Science, Research and Sport of the Slovak Republic under the Contract No. VEGA 1/0043/16 and by the grant of the Slovak Research and Development Agency under the Contract No. APVV-16-0186.

- [1] A. Gleizes and M. Verdaguer, *J. Am. Chem. Soc.* **103**, 7373 (1981).
- [2] M. Verdaguer, A. Gleizes, J.-P. Renard, and J. Seiden, *Phys. Rev. B* **29**, 5144 (1984).
- [3] E. Pardo, R. Ruiz-Garcia, F. Lloret, J. Faus, M. Julve, Y. Journaux, F. Delgado, and C. Ruiz-Perez, *Adv. Mater.* **16**, 1597 (2004).
- [4] S. W. Choi, H. Y. Kwak, J. H. Yoon, H. C. Kim, E. K. Koh, and C. S. Hong, *Inorg. Chem.* **47**, 10214 (2008).
- [5] S. Yamamoto, *Phys. Rev. B* **59**, 1024 (1999).
- [6] T. Sakai and S. Yamamoto, *J. Magn. Magn. Mater.* **226–230**, 645 (2001).
- [7] T. Sakai and K. Okamoto, *Phys. Rev. B* **65**, 214403 (2002).
- [8] A. S. Boyarchenkov, I. G. Bostrem, and A. S. Ovchinnikov, *Phys. Rev. B* **76**, 224410 (2007).
- [9] A. S. F. Tenório, R. R. Montenegro-Filho, and M. D. Coutinho-Filho, *J. Phys.: Condens. Matter* **23**, 506003 (2011).
- [10] J. Strečka, *Acta Phys. Polon. A* **131**, 624 (2017).
- [11] J. Strečka and T. Verkholyak, *J. Low Temp. Phys.* **187**, 712 (2017).
- [12] M. N. Leuenberger and D. Loss, *Nature (London)* **410**, 789 (2001).
- [13] A. Ardavan, O. Rival, J. J. L. Morton, S. J. Blundell, A. M. Tyryshkin, G. A. Timco, and R. E. P. Winpenny, *Phys. Rev. Lett.* **98**, 057201 (2007).
- [14] J.-F. Guo, X.-T. Wang, B.-W. Wang, G.-Ch. Xu, S. Gao, L. Szeto, W.-T. Wong, W.-Y. Wong, and T.-Ch. Lau, *Chem. Eur. J.* **16**, 3524 (2010).
- [15] X. Feng, T. D. Harris, and J. R. Long, *Chem. Sci.* **2**, 1688 (2011).
- [16] L. Bogani, L. Cavigli, K. Bernot, R. Sessoli, M. Gurioli, and D. Gatteschi, *J. Mater. Chem.* **16**, 2587 (2006).
- [17] M. Oshikawa, M. Yamanaka, and I. Affleck, *Phys. Rev. Lett.* **78**, 1984 (1997).
- [18] T. Sakai and S. Yamamoto, *Phys. Rev. B* **60**, 4053 (1999).
- [19] G.-H. Liu, L.-J. Kong, and J.-Y. Dou, *Solid State Commun.* **213–214**, 10 (2015).
- [20] M. Drillon, E. Coronado, R. Georges, J. C. Gianduzzo, and J. Curely, *Phys. Rev. B* **40**, 10992 (1989).
- [21] A. Caneschi, D. Gatteschi, and R. Sessoli, *Inorg. Chem.* **32**, 4612 (1993).
- [22] K. Fegy, D. Luneau, E. Belorizky, M. Novac, J.-L. Tholence, C. Paulsen, T. Ohm, and P. Rey, *Inorg. Chem.* **37**, 4524 (1998).
- [23] S.-S. Gong, W. Li, Y. Zhao, and G. Su, *Phys. Rev. B* **81**, 214431 (2010).
- [24] H. Miyasaka, T. Madanbashi, K. Sugimoto, Y. Nakazawa, W. Wernsdorfer, K. Sugiura, M. Yamashita, C. Coulon, and R. Clerac, *Chem. Eur. J.* **12**, 7028 (2006).
- [25] M. Balanda, M. Rams, S. K. Nayak, Z. Tomkowicz, W. Haase, K. Tomala, and J. V. Yakhmi, *Phys. Rev. B* **74**, 224421 (2006).
- [26] K. Bernot, L. Bogani, A. Caneschi, D. Gatteschi, and R. Sessoli, *J. Am. Chem. Soc.* **128**, 7947 (2006).
- [27] H. Wang, L.-F. Zhang, Zh.-H. Ni, W.-F. Zhong, L.-J. Tian, and J. Jiang, *Crystal Growth Design* **10**, 4231 (2010).
- [28] B. Bauer, L. D. Carr, H. G. Evertz, A. Feiguin, J. Freire, S. Fuchs, L. Gamper, J. Gukelberger, E. Gull, S. Guertler, A.



- Hehn, R. Igarashi, S. V. Isakov, D. Koop, P. N. Ma, P. Mates, H. Matsuo, O. Parcollet, G. Pawłowski, J. D. Picon *et al.*, *J. Stat. Mech.: Theory Exp.* (2011) P05001.
- [29] E. Lieb and D. Mattis, *J. Math. Phys.* **3**, 749 (1962).
- [30] Ö. Legeza and J. Sólyom, *Phys. Rev. Lett.* **96**, 116401 (2006).
- [31] S. J. Gu, G.-S. Tian, and H.-Q. Lin, *New J. Phys.* **8**, 61 (2006).
- [32] G.-H. Liu, H.-L. Wang, and G.-S. Tian, *Phys. Rev. B* **77**, 214418 (2008).
- [33] M. Dalmonte, J. Carrasquilla, L. Taddia, E. Ercolessi, and M. Rigol, *Phys. Rev. B* **91**, 165136 (2015).
- [34] Y.-Z. Huang and G. Su, *Phys. Rev. E* **95**, 052147 (2017).
- [35] W. Chen, K. Hida, and B. C. Sanctuary, *Phys. Rev. B* **67**, 104401 (2003).
- [36] A. Kitazawa, *J. Phys. A: Math and Gen.* **30**, L285 (1997).
- [37] S. J. Hu, B. Normand, X. Q. Wang, and L. Yu, *Phys. Rev. B* **84**, 220402(R) (2011).